Journal of the Oceanographical Society of Japan
Vol. 38, pp. 331 to 338, 1982

Internal Flow Structure of Short Wind Waves

Part III. Pressure Distributions*

Kuniaki OKUDA**

Abstract: For wind waves generated in a wind-wave tunnel, the surface pressure and also the pressure distribution along the internal streamlines were calculated from the measured internal velocity field. In distinct waves, with wave height comparable with or larger than the mean, the surface pressure is found to vary drastically in a narrow region around the crest, showing a dominant minimum near the crest. On the other hand, the pressure distribution along the streamline shows systematic variations that are nearly in phase with the streamline profile. It is shown that the occurrence of the pressure in phase with the streamline profile is linked with the internal vorticity distribution, especially with the presence of a high vorticity region below the crest described in Part I of this study. As a result of the occurrence of such pressure variations, the dispersion relation is modified by about 10 % from that for linear irrotational waves. It is argued from the present measurements that the dispersion relation and also the energy transfer from wind into wind waves are strongly affected by the internal vortical structure so that the assumption of irrotational gravity waves cannot be applied to the wind waves being studied.

1. Introduction

In Part I of this study (OKUDA, 1982a), characteristic features of the internal vorticity distribution relative to individual crests of short wind waves were described. For distinct waves with a wave height comparable with or larger than the mean, the surface vorticity layer was found to be greatly thickened near the crest where vorticity is particularly high. In Part II (OKUDA, 1982b), the influence of this high vorticity region on the overall internal flow field of individual waves was discussed, and it was found that the internal streamline pattern of wind waves differs significantly from that predicted for irrotational water waves. In this paper characteristic features of the pressure field relative to individual crests are described, and the manner of coupling between the wind and wind waves having particular internal vortical structures as descrived in Part I (OKUDA, 1982a), is discussed.

LONGUET-HIGGINS (1969) interpreted the effect of varying tangential stress on wave growth by estimating the additional pressure arising on a streamline just below the surface vorticity layer. By use of his idea of separating the inner region from the surface vorticity layer, an important aspect of wind-wave coupling is revealed as follows. The measurements described in Part II showed that a regular wave motion dominates in the inner region below the surface vorticity layer in spite of the presence of the high vorticity region below the crest. If the high verticity region is not supported steadily but repeatedly grows and attenuates in individual waves as mentioned in Part II, it follows that only that part of the energy flux from wind into wind waves which supports the growth of wave motion in the inner region is retained persistently in wind waves. This implies that the substantial part of wind wave motion lies in the inner irrotational wave motion. The wave motion in the inner region is constrained by the kinematical and dynamical conditions at the streamlines which pass just below the surface vorticity layer, for example η' shown in fig. 6 in Part II (OKUDA, 1982b), so that the dispersion relation and the wind wave growth are governed by the pressure distribution along η' which is a consequence of the dynamics in the surface vorticity layer. The influence of surface pressure and surface tangential stress on wind wave

* Received Mar. 6, 1981, revised Apr. 28 and accepted May 25, 1982.

** Geophysical Institute, Faculty of Science, Tohoku University, Sendai 980, Japan

dynamics thus appears indirectly in the pressure distribution along η'. It can be said that wind waves are coupled with the wind through the buffer of the surface vorticity layer.

In later sections of the present paper pressure distributions along the streamlines which pass through the inner irrotational region and also the surface pressure distributions are shown. They indicate that the pressure distribution along the interior streamline is affected by the presence of the high vorticity region, and differs greatly from the surface pressure distribution. Results of the present study illustrate the complexity of the dynamics of the short wind waves being studied.

2. Method of calculation of the internal pressure field

The flow of the wind waves studied was approximately two-dimensional, and, for four waves in the field, the internal velocity field, which was smoothed by removing irregular variations with horizontal scales much smaller than the wavelength, has already been measured (sect. 2 in Part I: OKUDA, 1982a). The internal pressure field can be obtained from the measured velocity field as follows. We assume that the small scale turbulent motion is not intense and the flow of wind waves is steady in a frame of reference moving with the wave profile (x, z), where horizontal axis (x) is positive downwind and vertical axis (z) is positive upward. The equations for U (x-component velocity) and W (z-component velocity) under the above assumptions are

$$-C\frac{\partial U}{\partial x}+U\frac{\partial U}{\partial x}+W\frac{\partial U}{\partial z}+g\frac{\partial \eta}{\partial x}=-\frac{1}{\rho}\frac{\partial \hat{P}'}{\partial x} \quad (1)$$

$$-C\frac{\partial W}{\partial x}+U\frac{\partial W}{\partial x}+W\frac{\partial W}{\partial z}=-\frac{1}{\rho}\frac{\partial \hat{P}'}{\partial z}, \quad (2)$$

where ρ is the density of water, g is the gravitational acceleration, η is the surface displacement, C is the phase speed, and $\hat{P}'$ is the pressure corrected for hydrostatic pressure. By integrating Eqs. (1) and (2), we obtain the pressure at an arbitrary point (x_1, z_1), except an integral constant $\hat{P}'$ (x_0, z_0), as

$$\begin{aligned}\hat{P}(x_1, z_1)&\equiv\hat{P}'(x_1, z_1)-\hat{P}'(x_0, z_0)\\&=\rho\left[\int_{x_0}^{x_1}C\frac{\partial U}{\partial x}dx\right]_{z=z_0}+\rho\left[\int_{z_0}^{z_1}C\frac{\partial W}{\partial x}dz\right]_{x=x_1}\\&\quad-\rho\left[\int_{x_0}^{x_1}\left(U\frac{\partial U}{\partial x}+W\frac{\partial U}{\partial z}\right)dx\right]_{z=z_0}\\&\quad-\rho\left[\int_{z_0}^{z_1}\left(U\frac{\partial W}{\partial x}+W\frac{\partial W}{\partial z}\right)dz\right]_{x=x_1}\\&\quad-\rho g\{\eta(x_1)-\eta(x_0)\}\end{aligned} \quad (3)$$

where $[\ ]_{z=z_0}$, for example, indicates the value at $z=z_0$. The integrations were performed by using the measured velocity field, and it was confirmed that the calculated pressure distributions were independent of the integration path.

There may be errors in the calculated pressure distribution due to the following:

(a) the assumption of the two dimensionality of the flow and the exclusion of the effect of turbulence,

(b) errors in the measurement of the flow velocity and the wave profile,

(c) time fluctuations of the wave profile and the internal flow patterns during propagation of the wave.

However, only the error introduced in relation to determination of the overall wave profile is significant (OKUDA, 1980). As mentioned in Part I (OKUDA, 1982a), the error in the determination of overall wave profiles is 0.2 mm, corresponding to an error in pressure of 20 dyne cm^{-2}.

The calculated pressure fields $\hat{P}$ $(=P+\rho g\eta)$ are shown in Fig. 1. For Case I the air friction velocity (u_*) is 46 cm s^{-1} and the fetch (F) is 3 m, and for the other cases (Cases II~IV: Fig. 1b~d) u_* is 30 cm s^{-1} and F is 6 m; the details of experimental conditions and characteristic values of the four waves have been described in Part I (OKUDA, 1982a: sect. 2.1). The numbers on the contours are the pressure in dyne cm^{-2}. From the calculated internal pressure fields, together with the streamline patterns shown in fig. 1 in Part II (OKUDA, 1982b), the pressure distributions along the streamlines were obtained and the surface pressure distributions were obtained by extrapolating the internal pressure field linearly up to the water surface.

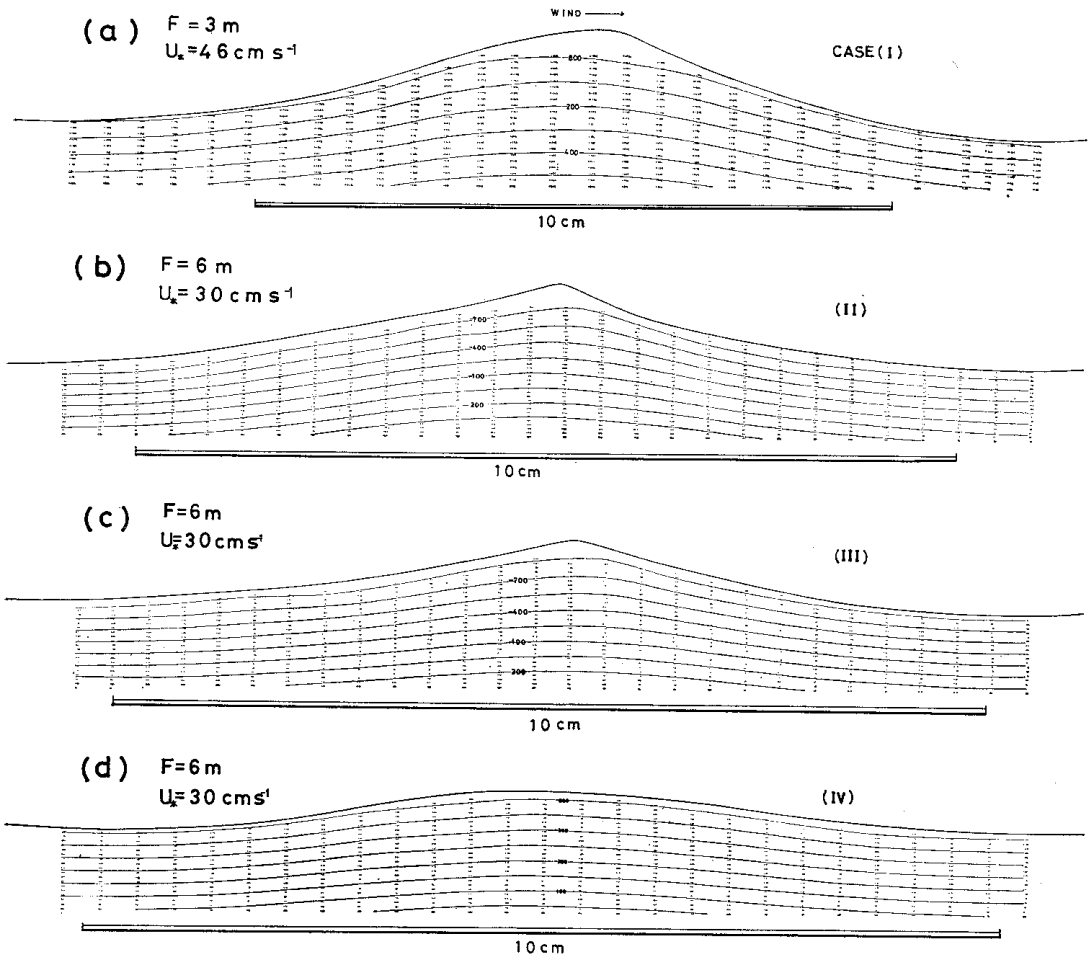

Fig. 1. Pressure field calculated from the internal flow field. Numbers on the lines in each figure represent the pressure (dyne cm^{-2}) with reference to a fixed value. For Case I shown in (a) the air friction velocity (u_*) is 46 cm s^{-1} and the fetch (F) is 3 m, and for Cases II, III and IV shown in (b), (c) and (d), respectively, u_* is 30 cm s^{-1} and F is 6 m.

3. Results and discussion

3.1. Pressure variations along the streamline

The pressure distributions along the streamlines which pass through the inner irrotational region below the surface vorticity layer are shown in Fig. 2. The streamlines treated here and the streamlines shown in fig. 1 in Part II (OKUDA, 1982b) can be identified from the value of the stream function Ψ (cm^2 s^{-1}). Open circles connected by the solid lines indicate the periodic part, and the inclined dash-dot lines the uniform drift. The streamline profiles are indicated by thin solid lines. Except for Case II the drift is distinct. As shown in Part II (OKUDA, 1982b: sect. 4.2), measured streamlines contained some vertical drift, presumably produced by large-scale turbulent motion and also the non-uniformity of the wave train. The pressure drift is associated with the streamline drift.

The periodic parts, except for $\Psi=0$ and -10 in Case IV, show variations nearly in phase with the streamline profiles. In particular, those for Cases I and II show quite distinct variations; the ranges of variations exceed four times the maximum error (20 dynes cm^{-2}). For Cases I, III and IV, phase differences between the pressure and the streamline profile can be found. Such phase differences, however, may not be significant considering the presence of the drift mentioned above and the errors in the pressure

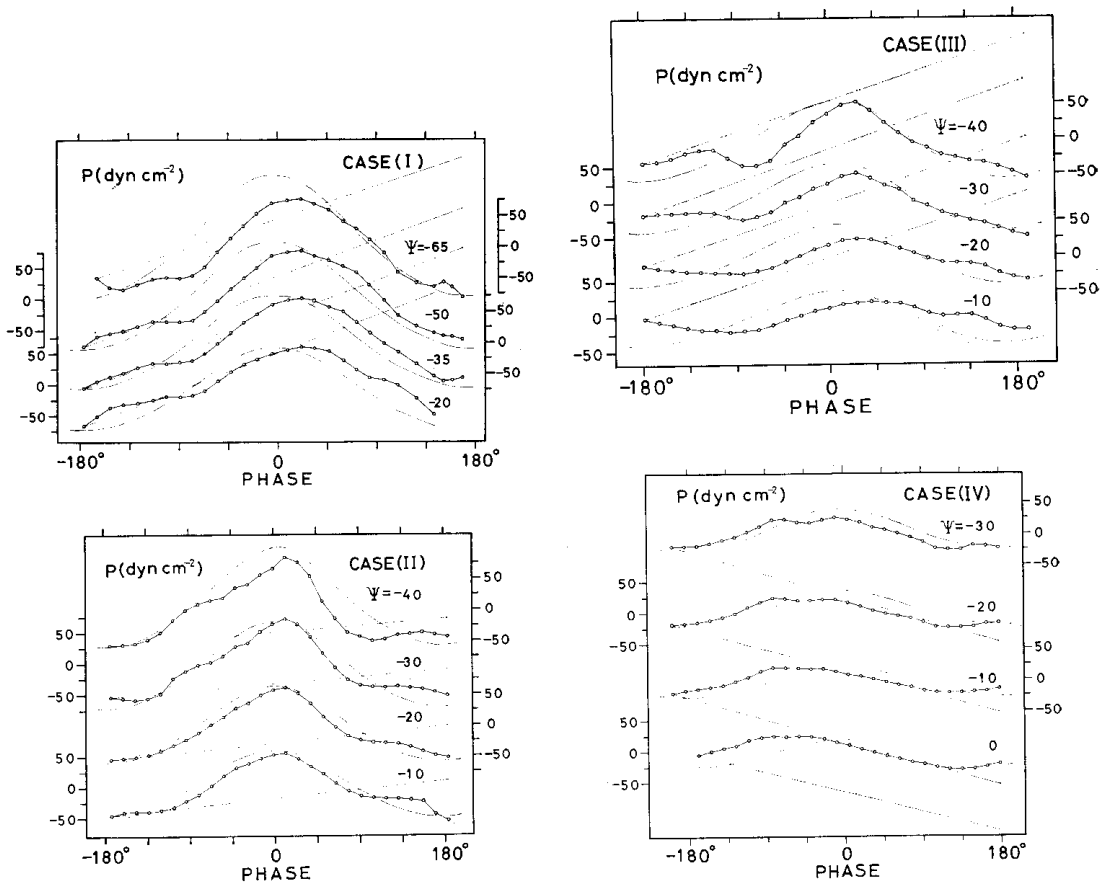

Fig. 2. Pressure distributions along streamlines. Open circles represent the periodic part and inclined dash-dot lines the uniform drift. Thin solid curves represent the respective streamline profiles.

measurements; the ranges of the pressure variations for $\Psi=-20$ and -10 in Case III and $\Psi=0$ and -10 in Case IV, in which the phase difference is distinct, may not be large enough compared with the possible error to be significant.

The occurrence of pressure variations in phase with the streamline profile for distinct waves (Cases I, II and III) can be interpreted as follows. As shown in Part II (OKUDA, 1982b: sect. 3), the streamlines below the surface vorticity layer pass approximately along the lines of equal vorticity, not along the water surface. This implies that a pressure roughly comparable with the weight of water in the high vorticity region near the crest is imposed additionally on the wave motion in the inner region. The typical thickness of the high vorticity region at the crest was about $0.35H$, where H is the wave height, for Cases I, II and III (OKUDA, 1982b: sect. 4.2), which suggests that pressure variations of about $0.35\rho gH$ arise. It is thus evident that the pressure variations in phase with the streamline profile are associated mainly with the presence of the high vorticity region near the crest, though the effect is reduced considerably by the surface pressure variations which will be shown in Section 3.2.

From the measurements of the pressure distributions along the steamline for Cases I, II and III, we can discuss the influence of the presence of the high vorticity region on the dispersion relation. Let us assume that the pressure variations for Cases I, II and III shown in Fig. 2 are in phase with streamline profile with an amplitude

$$P_a=\Delta P/2\,,$$

where ΔP is the range of variations. Every

streamline treated here passes, in most parts, through the region where the flow is substantially irrotational, and the steepness of all streamline profiles is small. Thus, the dispersion relation can be obtained simply as follows. To a first-order approximation, the dynamical and the kinematical boundary conditions at $z=\bar{z}_\Psi$, where $\bar{z}_\Psi$ is the mean depth of a streamline, are respectively

$$\frac{P_\Psi}{\rho}+g\eta_\Psi+\frac{\partial\phi}{\partial t}=0, \qquad (4)$$

$$\frac{\partial\eta_\Psi}{\partial t}=\frac{\partial\phi}{\partial z}, \qquad (5)$$

where P_Ψ is the pressure on the streamline under consideration, η_Ψ is the vertical displacement around $\bar{z}_\Psi$ and ϕ is the velocity potential. Since P_Ψ is in phase with η_Ψ, it can be expressed as

$$P_\Psi=P_a\eta_\Psi/a \qquad (6)$$

where a is the amplitude of the streamline. From Eqs. (5) and (6),
Eq. (4) is rewritten as

$$\frac{\partial^2\phi}{\partial t^2}+\left(g+\frac{P_a}{\rho a}\right)\frac{\partial\phi}{\partial z}=0 \qquad (7)$$

By assuming $\phi\propto e^{kz}\sin(kx-\sigma' t)$, we obtain the dispersion relation

$$\sigma'=\sigma\left(1+\frac{P_a}{\rho g a}\right)^{1/2}$$

where $\sigma=(gk)^{1/2}$.

The values of σ'/σ calculated for respective streamlines and also the values of P_a and a are summarized in Table 1. The dispersion relation is modified by about 10 % from that for linear irrotational waves with constant surface pressure. In Part II (OKUDA, 1982b: sect. 4.2) it was shown that the amplitude of the velocity distribution along the streamline is larger than $a\sigma$ by about 12 %, which is consistent with the present result. In this table the observed phase speed is also compared with σ'/k. They differ slightly. However, the reason for this is quite clear. A rather uniform flow exists in the inner region of respective waves as shown in fig. 7 in Part II (OKUDA, 1982b). Individual waves are not only forced by the pressure distribution which is in phase with the streamline profile but are also advected by such uniform flow. The advection speed is known to be 4-5 cm s^{-1} for Case I and 2-3 cm s^{-1} for Cases II and III from the same figure (OKUDA, 1982b: fig. 7). The observed phase speeds can be interpreted by taking such advection into consideration. It should be noted that it is not possible to estimate the effect of the rotational motion on the phase speed simply by assuming the existence of a drift current with a definite profile and surface velocity, as HIDY and PLATE (1966) and KELLER *et al.* (1975) did, because in the wind waves being studied the thickness of the surface vorticity layer and also the value of vorticity vary greatly along the wave profile so that this assumption is unrealistic.

3.2. Surface pressure variations

Figure 3 shows the surface pressure P_s, to-

Table 1. Calculated values of σ'/σ and the values of the phase speed measured and calculated.

		a (cm)	P_a (dyne cm^{-2})	σ'/σ	C (cm s^{-1}) obs.	σ'/k
Case I	$\Psi=-65$	0.49	75	1.08		
	-50	0.43	75	1.09	57.4	54.0
	-35	0.37	71	1.09		
	-20	0.33	64	1.09		$\sigma'/\sigma=1.09$
Case II	$\Psi=-40$	0.30	70	1.11		
	-30	0.26	64	1.12	51.0	48.2
	-20	0.23	57	1.12		
	-10	0.20	52	1.12		$\sigma'/\sigma=1.12$
Case III	$\Psi=-40$	0.21	51	1.12		
	-30	0.18	39	1.11	47.0	44.6
	-20	0.16	28	1.09		
	-10	0.14	21	1.07		$\sigma'/\sigma=1.10$

gether with the wave profile η. The open circles connected with solid lines show the distributions obtained by linear extrapolation of the interior profiles. The errors introduced by the extrapolation are generally negligibly small, but near the crest for Cases I, II and III, for which the flow measurements are not available within a few millimeters below the water surface, they may not necessarily be small. At some points near the crest for Cases I, II and III, the surface pressure was estimated not only by linear extrapolation but also by calculating the pressure near the crest on the basis of the predicted flow pattern from the investigations of Parts I and II of this study (OKUDA, 1982a, b); the details of this method are described in OKUDA (1980). The distributions obtained by this method are shown by solid circles connected with dashed lines. The inclined dash-dot lines for Cases II and IV indicate the drift. It should be noted that the possible error of 20 dynes cm^{-2} in the present measurements is too large to detect the pressure drag $\overline{P_s \frac{\partial \eta}{\partial x}}$, i.e. the mean horizontal component of the pressure acting on the water surface. In the following part of this section the main patterns in the measured pressure distributions are described.

The distributions for Cases I, II and III show pronounced variations in a narrow region near the crest ($-40°\sim30°$), with a distinct minimum at a point very close to the crest. The ranges of variations are far beyond the extent of possible error. This feature is found in neither the measurements by KENDALL (1970) over a wavy wall nor in those of SHEMDIN and HSU (1967) over mechanically generated waves; the ranges of overall pressure variations are comparable with KENDALL (1970)'s corresponding measurements, but are one order of magnitude larger than those of SHEMDIN & HSU at a corresponding wind speed. A similar pressure variation is also found in Case IV, although the pressure minimum a little to the rear of the crest is not so distinct as in Cases I, II and III. This feasure in the surface pressure distribution corresponds well to the presence of distinct maxima in the tangential stress distributions (OKUDA, 1982a: fig. 7), and may be associated with the strong air flow as a jet near the crest, as suggested by CHANG *et al.* (1971).

In Part I (OKUDA, 1982a: sect. 3.2) it was shown that the surface velocity of short wind waves is not small compared with the phase speed, and for distinct waves, in particular, it is in excess of the phase speed. The numerical

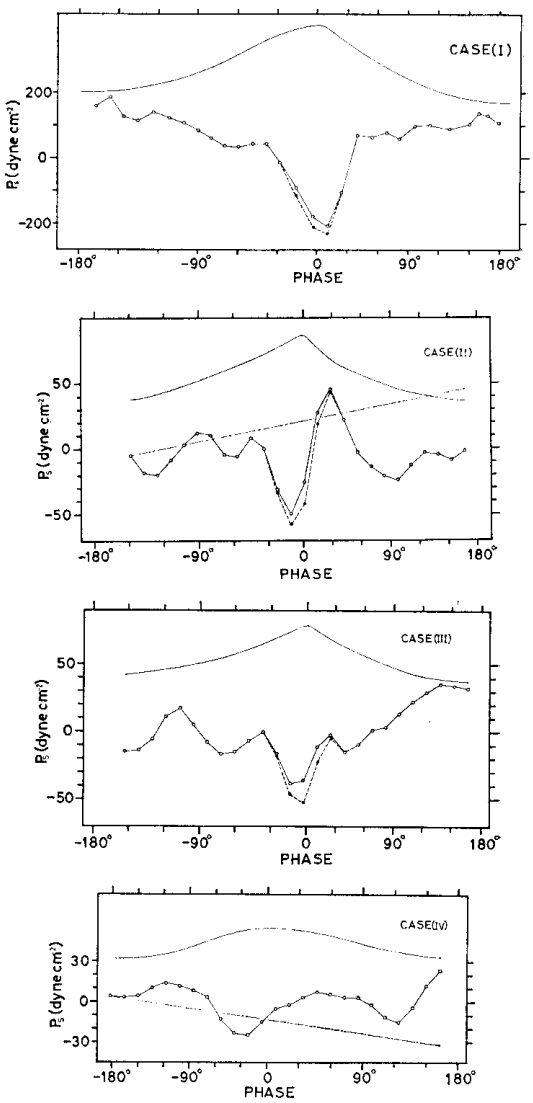

Fig. 3. Distributions of the surface pressure. The open circles connected with solid lines show the distributions obtained by linear extrapolation of the interior profiles. The solid circles connected with dashed lines near the crest for Cases I, II and III represent the corrected distributions. The inclined dash-dot lines in Cases II and IV represent the pressure drift. The wave profiles are shown by solid curves. The phase is defined as 0° at the crest.

study by GENT and TAYLOR (1977) suggests that the distinct minimum in the surface pressure is associated with such kinematical conditions at the water surface. Their calculations for a wave with small steepness and a surface velocity much smaller than the phase speed show regular sinusoidal variations of both the pressure and the tangential stress. On the other hand, the stress distributions for waves with large steepness and a surface velocity close to the phase speed show similar patterns to the present measurements, though the ranges of measured stress distributions for Cases I, II and III are 3–5 times larger than their calculations.

The pressure distributions near the crest show a noticeable difference between Case II and Case III. This might be associated with the occurrence of air flow separation in Case II and its absence in Case III, which was discussed in Part I (OKUDA, 1982a: sect. 3.1). The distribution for Case II shows a distinct asymmetry with respect to the crest, unlike Case III (and also Case I). In Case II a maximum occurs a little leeward of the crest (about 30°) and the value at this point is larger than that a little windward of the crest (about −40°) by about 40 dyne cm^{-2}. This indicates that a net adverse pressure is acting locally on the crest, below which the high vorticity region occurs; the occurrence of such a pressure distribution may not necessarily contradict the well-known fact that air flow separation increases the pressure drag, since the pressure drag is related to the overall distributions along the wave profile. In Part II (OKUDA, 1982b: sect. 4.1) the characteristics of flow in the high vorticity region for Case II were discussed on the basis of the measured vorticity distribution and the streamlines, and it was pointed out that a net leakage of water out of the high vorticity region occurs, and the steepness of the crest decreases. Such features of flow near the crest may be associated with the net adverse pressure acting on the crest found here.

4. Concluding remarks

By comparing the surface pressure and the pressure distribution along streamlines of wind waves for three cases (I, II and III), it is seen that the features in the former completely disappear in the latter. The overall surface pressure distributions are out of phase with the wave profiles (see Fig. 3), whereas the pressure distributions along the streamlines are in phase with the streamline profile (see Fig. 2). The occurrence of such distinct differences is associated with the presence of a high vorticity region below the crest. In Section 3.1 the dispersion relation was determined from the pressure distribution along the interior streamline. If the dispersion relation had been determined from the surface pressure under the assumption that the wind waves being studied are irrotational, invalid results would have been obtained.

The growth of wind waves being studied is also influenced by the internal vortical structure. The energy flux from wind into wind waves, including the effect of tangential stress $\overline{\tau' U_s'}$ described in Part I (OKUDA, 1982a), is given by $f=\overline{\tau' U_s'}-\overline{P_s W_s}$, where τ' and U_s' are the fluctuating parts of the tangential stress and the horizontal component of surface velocity, respectively, and W_s is the vertical component of surface velocity. In the case of substantially irrotational waves, f can be estimated immediately from the stress distributions at the water surface, since U_s' and W_s can be approximated by the horizontal and the vertical components of the orbital velocity, respectively. However, in the wind waves being studied the surface velocity distribution is strongly affected by the existence of the high vorticity region as shown in Part I (OKUDA, 1982a: fig. 7). Furthermore, in the present case, f does not entirely support the growth of wind waves. The internal flow of wind waves is accompanied by the strong velocity shear especially in the high vorticity region below the crest. The intrusion of water elements a little leeward of the crest (the wave breaking in a wide sense) occurs in some waves, and in such waves the high vorticity region attenuates, as noted in Part II (OKUDA, 1982b: sect. 4.1). The above facts suggest that a considerable part of f is dissipated. The energy flux which contributes to the wind wave growth thus is $\tilde{f}=f-D$ where D is the dissipation.

Consideration of the above indicates that f, D and, subsequently, $\tilde{f}$ are strongly dependent on the flow in the surface vorticity layer. This may also be seen from the alternative expression $\tilde{f}=-\overline{P_{\eta'} W_{\eta'}}$, where $P_{\eta'}$ and $W_{\eta'}$ are the pres-

sure and the vertical component of flow velocity, respectively, at a streamline just below the surface vorticity layer (for example, η' shown in fig. 6 in Part II: OKUDA, 1982b). The measurements described in this paper and in Part II (OKUDA, 1982b) indicate that the internal pressure field and also the internal flow pattern are strongly affected by the occurrence of the high vorticity region below the crest. This shows that the growth of short wind waves cannot be clarified without an appropriate understanding of the dynamics of the internal vortical structure.

References

CHANG, P. C., E. J. PLATE and G. M. HIDY (1971): Turbulent air flow over the dominant component of wind-generated water waves. J. Fluid Mech., **47**, 183-208.

GENT, P. E. and P. A. TAYLOR (1977): A note on 'separation' over short wind waves. Boundary-Layer Meteorology, **11**, 65-87.

HIDY, G. M. and E. J. PLATE (1966): Wind action on water standing in a laboratory channel. J. Fluid Mech., **26**, 651-687.

KELLER, W. C., T. R. LARSON and J. W. WRIGHT (1974): Mean speeds of wind waves at short fetch. Radio Sci., **9**, 1091-1100.

KENDALL, J. M. (1970): The turbulent boundary layer over a wall with progressive surface waves. J. Fluid Mech., **41**, 259-281.

LONGUET-HIGGINS, M. S. (1969): Action of a variable stress at the surface of water waves. Phys. Fluids, **12**, 737-740.

OKUDA, K. (1980): Study on the internal structure of wind waves. Doctoral thesis, Tohoku Univ., 145 pp.

OKUDA, K. (1982a): Internal flow structure of short wind waves. Part I. On the internal vorticity structure. J. Oceanogr. Soc. Japan, **38**, 28-42.

OKUDA, K. (1982b): Internal flow structure of short wind waves. Part II. The streamline pattern. J. Oceanogr. Soc. Japan, **38**, 313-322.

SHEMDIN, O. H. and E. Y. HSU (1967): The dynamics of wind in the vicinity of progressive water waves. J. Fluid Mech., **30**, 403-416.

発達初期の風波の内部構造

第3報　圧力分布について

奥　田　邦　明*

要旨: 測定した個々波内部の流速場から，水面に沿った圧力分布，及び内部の流線に沿った圧力分布を計算した．平均以上の波高を持つ場の代表的な波について，水面圧力は峯付近で急激に減少し顕著な最小値を持つこと，そして内部の流線に沿った圧力は，水面圧力とは逆の，変位と同位相の規則的な変化を示すことが解った．内部の流線に沿った変位に同位相の圧力変化は，第1報で示した個々波内部の渦度分布，特に峯付近の高渦度領域の存在に起因していること，そして風波の分散関係は，このような内部の圧力場の形成に伴い，渦なし線形波のそれから約 10％ 違っていることが解った．ここで見い出された水面圧力分布と内部の流線に沿った圧力分布との顕著な相違は，風波の力学に内部の渦度構造が決定的な影響を及ぼしており，発達初期の風波に対して，非回転波動の仮定を適用することができないことを示している．

* 東北大学理学部　〒980 仙台市荒巻字青葉